Materials Transactions, Vol. 45, No. 7 (2004) pp. 2122 to 2127
Special Issue on Grain Boundaries, Interfaces, Defects and Localized Quantum Structures in Ceramics

High Temperature Deformation Behavior of [0001] Symmetrical Tilt $\Sigma 7$ and $\Sigma 21$ Grain Boundaries in Alumina Bicrystals

Satoru Hanyu[1,*1], Hitoshi Nishimura[1,*1] Katsuyuki Matsunaga[2,*2]
Takahisa Yamamoto[3], Yuichi Ikuhara[2] and Taketo Sakuma[3]

[1]*Department of Materials Science, School of Engineering, The University of Tokyo, Tokyo 113-8656, Japan*
[2]*Institute of Engineering Innovation, The University of Tokyo, Tokyo 113-8656, Japan*
[3]*Department of Advanced Materials Science, Graduate School of Frontier Sciences, The University of Tokyo, Tokyo 113-8656, Japan*

High temperature deformation behavior of [0001] symmetrical tilt grain boundaries of Al_2O_3 was investigated by using bicrystals. Four kinds of the grain boundaries $\Sigma 7/\{4\bar{5}10\}$, $\Sigma 21/\{4\bar{5}10\}$, $\Sigma 7/\{2\bar{3}10\}$ and $\Sigma 21/\{2\bar{3}10\}$ were selected in the present study, and compressive mechanical tests were performed at 1450°C in air to investigate the sliding behavior of the respective boundaries. It was found that, stresses readily increased with increasing strains for all specimens during compression tests, but the bicrystals showed abrupt sliding along the grain boundary planes to fracture. Among the boundaries studied, $\Sigma 7/\{4\bar{5}10\}$ exhibited the highest resistance to the grain boundary sliding. The other boundaries showed similar sliding resistance, and yet the stress and strain values at their failure were much smaller than those of $\Sigma 7/\{4\bar{5}10\}$. In order to understand the mechanism of the sliding behavior of the respective boundaries, the grain boundary core structures and their atomic densities were examined, based on the structure models obtained in our previous studies. It was found that $\Sigma 7/\{4\bar{5}10\}$ having the highest sliding resistance showed a larger atomic density at the core, as compared to the others. Therefore, the observed sliding resistance of the boundaries is closely related to the detailed atomic structures at the grain boundary cores.

(Received January 30, 2004; Accepted April 21, 2004)

Keywords: *alumina, bicrystal, transmission electron microscopy, grain boundary structure, grain boundary sliding*

1. Introduction

Polycrystalline alumina (Al_2O_3) is an important structural material at high temperatures. To control its mechanical property is necessary for practical use of alumina. It has been reported that macroscopic properties of polycrystalline alumina strongly depend on grain boundary properties. For example, high-temperature deformation of fine-grained alumina ceramics is controlled by grain boundary sliding and diffusion[1,2] and is influenced by impurities segregating at grain boundaries.[3–5] It is very important to understand the relationships between grain boundary characters and their properties in alumina.

Since polycrystalline alumina has many grain boundaries with different properties, it is necessary to systematically clarify the atomic structures of individual grain boundaries to investigate properties of alumina ceramics due to grain boundaries. Bicrystal experiment is very effective to study the relationship among grain boundary characters, structures and properties, because grain boundaries with given misorientations and inclination of grains can be artificially controlled. So far bicrystal experiments have been adopted to investigate grain boundary structures and mechanical properties for metals[6–10] according to the coincidence site lattice (CSL) theory.[11] In the CSL theory, the CSL lattice is determined by a rotation axis and a rotation angle, and Σ values for grain boundaries can be defined as the degree of geometrical matching between two adjacent crystals. It was found that atomic structures, energies and mechanical properties of symmetrical grain boundaries are dependent on grain boundary characters. For example, in tilt grain boundaries of metals, deep grain boundary energy cusps are often observed for special grain boundaries with relatively small Σ values. And it was reported that grain boundary sliding was hard to occur at small Σ grain boundaries, compared to larger Σ grain boundaries.[6]

Although bicrystal experiments for ceramics are fewer than for metals, several bicrystal studies have been performed for MgO,[12] TiO_2,[13,14] NiO,[15] ZrO_2,[16–18] and Al_2O_3[19–28] to reveal the detailed atomic structures and energies of specific grain boundaries. For alumina, atomic structures of the grain boundaries have been studied by high-resolution transmission electron microscopy (HRTEM), and also have been analyzed by using a static lattice calculations.[26,31,32] A number of experiments have revealed the importance of grain boundary planes for grain boundary structures and energies, although Σ parameters are often used to understand the stability of grain boundaries.[29–32] But, a correlation between atomic structures and mechanical properties of the grain boundary has not been investigated in detail.

In this study, relationships between sliding behavior and grain boundary atomic structures were investigated for four types of symmetrical tilt grain boundaries, *i.e.*, $\Sigma 7/\{4\bar{5}10\}$, $\Sigma 21/\{4\bar{5}10\}$, $\Sigma 7/\{2\bar{3}10\}$ and $\Sigma 21/\{2\bar{3}10\}$ in alumina bicrystals. These boundaries have different Σ values with the same grain boundary plane, otherwise it can be said that they have the same Σ value with different grain boundary planes. Compression tests were performed to investigate the grain boundary (G.B.) sliding behavior for using the grain boundaries, and the obtained results were discussed with the detailed core structures of the respective grain boundaries.

*1Graduate Student, The University of Tokyo
*2Corresponding author, E-mail: matu@sigma.t.u-tokyo.ac.jp

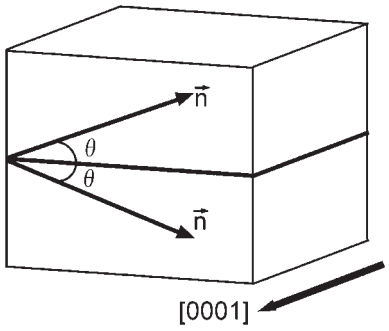

Fig. 1 Schematic illustration of the fabricated alumina bicrystal which have [0001] tilt grain boundary with a misorientation angle "2θ".

Table 1 Crystallographic parameters for fabricated alumina bicrystals.

$\vec{n}$	2θ (Σ value)		G.B. plane
$[1\bar{1}00]$	38.2°	($\Sigma 7$)	$\{4\bar{5}10\}$
$[1\bar{1}20]$	38.2°	($\Sigma 7$)	$\{2\bar{3}10\}$
$[1\bar{1}20]$	21.8°	($\Sigma 21$)	$\{4\bar{5}10\}$
$[1\bar{1}00]$	21.8°	($\Sigma 21$)	$\{2\bar{3}10\}$

2. Experimental Procedures

2.1 Fabrication of Al_2O_3 bicrystals

High purity (>99.99%) α-Al_2O_3 single crystals were used to fabricate alumina bicrystals. They were cut with a size of $6 \times 12 \times 15\,mm^3$ by a diamond saw. Their surfaces corresponding to grain boundary planes were mechano-chemically polished using colloidal silica to obtain a mirror state. Two single crystals with mirror state surfaces were jointed by a diffusion bonding method at 1500°C, for 10 h in air. The size of the bicrystals thus obtained was $12 \times 12 \times 15\,mm^3$. The bicrystals fabricated in this study contain [0001] symmetrical tilt grain boundaries of $\Sigma 7/\{4\bar{5}10\}$, $\Sigma 21/\{4\bar{5}10\}$, $\Sigma 7/\{2\bar{3}10\}$ and $\Sigma 21/\{2\bar{3}10\}$. Figure 1 and Table 1 show tilt angles 2θ between the $\boldsymbol{n}$ direction, Σ values, and grain boundary planes for the respective boundaries, where $\boldsymbol{n}$ corresponds to the $[1\bar{1}00]$ or $[11\bar{2}0]$ direction.

2.2 Compression test

Grain boundary sliding in Al_2O_3 bicrystals was investigated by compression tests. The compression tests were carried out at 1450°C, in air, where a constant strain rate of $\dot{\varepsilon} = 2.1 \times 10^{-6}\,s^{-1}$ was employed. Specimens for the compression test were cut out with the size of $4 \times 4 \times 8\,mm^3$ from each bicrystal (Fig. 2). In the specimens, the grain boundary planes were set to incline by 45° with respect to the compression axis so as to apply maximum shear stresses to the grain boundary. In this case, the (0001) plane was set parallel to the compression axis so as not to activate basal slip, which is the primary slip system at high temperatures in alumina. Scratched lines were introduced on (0001) surfaces of the specimen, to investigate the amount of the grain boundary sliding due to the compression tests. For the $\Sigma 7/\{4\bar{5}10\}$ and $\Sigma 21/\{4\bar{5}10\}$ boundaries, compression tests were conducted under the same conditions, and were interrupted several times before fracture occurs. At each interruption, the morphology of the grain boundaries was observed by an optical microscope.

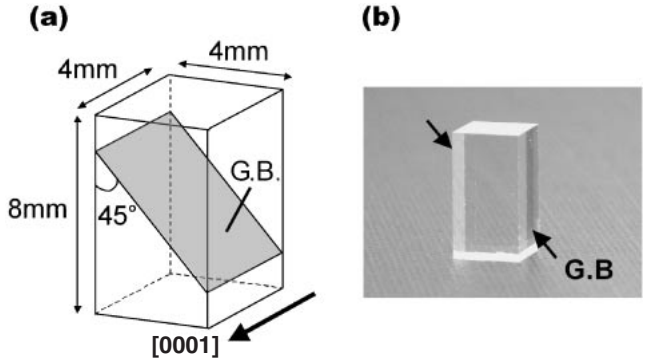

Fig. 2 (a) Schematic illustration of the specimen for compression tests cut out from fabricated alumina bicrystals.

2.3 HRTEM observations and Calculation

Grain boundaries were observed by transmission electron microscopy (TEM) to investigate their grain boundary structures. Specimens were prepared from the fabricated bicrystals by ion thinning method. High resolution TEM (HRTEM) observations were performed by the Topcon EM-002B, TEM at 200 kV with a point-to-point resolution of 0.18 nm. Grain boundaries were observed in a cross sectional view parallel to the [0001] direction. Static lattice calculations were performed by using the GULP code[33] to analyze atomic structures of grain boundaries in bicrystals.[31,32]

3. Results and Discussion

Figure 3 shows the stress-strain curves obtained from the compression tests in this study. It was found that stress readily increased with increasing strain for all specimens during compression tests, and $\Sigma 7/\{4\bar{5}10\}$ exhibited the highest fracture stress among these grain boundaries. The other boundaries showed different fracture stresses with one another, and yet the stress and strain values at their fracture were much smaller than those of $\Sigma 7/\{4\bar{5}10\}$. It was also confirmed that the fracture occurred along the grain boundary planes in the bicrystals, and thus the fracture stress is considered to correspond to the grain boundary sliding resistances. It should be noted here that the $\Sigma 7/\{4\bar{5}10\}$ and $\Sigma 7/\{2\bar{3}10\}$ boundaries have the same Σ value, but their sliding resistances were quite different. Therefore, the degree of the sliding resistances can not be simply understood by the geometrical coherency expressed by the Σ values.

Figure 4 shows optical micrographs of the surface morphology for the (a) $\Sigma 7/\{4\bar{5}10\}$ G.B. deformed up to $\varepsilon = 1.3\%$ (137.5 MPa), and (b) $\Sigma 21/\{4\bar{5}10\}$ G.B. deformed up to $\varepsilon = 0.7\%$ (37.5 MPa). Although the grain boundaries were initially straight before compression tests, the grain boundary lines exhibited a zig-zag shape, indicating G.B. migration took place in both boundaries during the compression tests. It should be noted, however, that from the gaps between scratched lines, G.B. sliding was apparently observed at the $\Sigma 21/\{4\bar{5}10\}$ grain boundary even at such a small stress, while G.B. sliding did not explicitly occur at the $\Sigma 7/\{4\bar{5}10\}$ grain boundary, nevertheless of such a high applied stress. It is noted that a size of zig-zag shape of $\Sigma 7/\{4\bar{5}10\}$ is rather

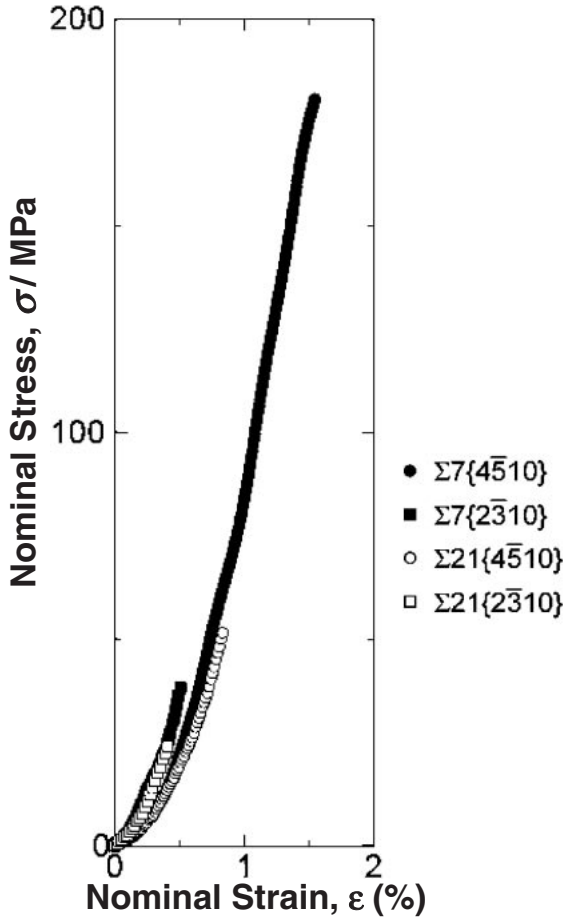

Fig. 3 Stress-strain curves obtained for the respective specimens by the compression tests at 1450°C in air.

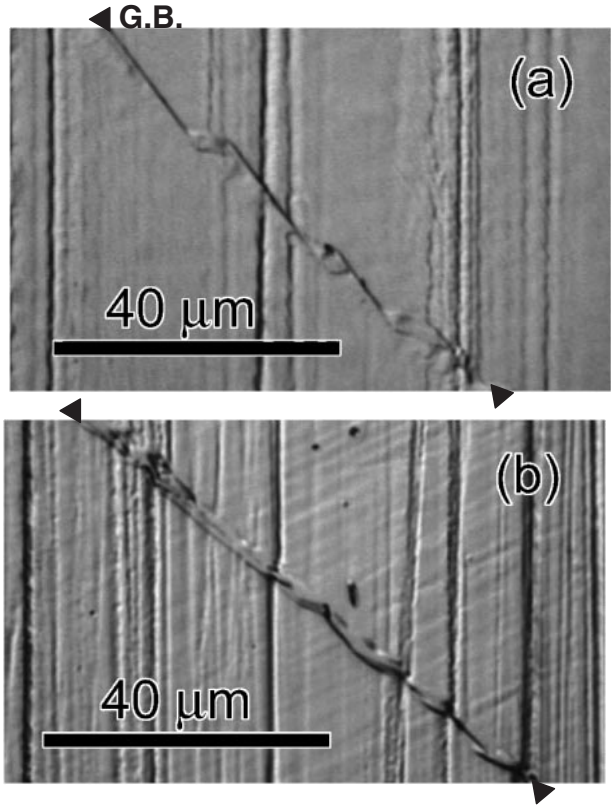

Fig. 4 Optical micrographs of the (a) $\Sigma 7$ {4$\bar{5}$10} specimen deformed up to $\varepsilon = 1.3\%$ ($\sigma = 137.5$ MPa) and (b) $\Sigma 21$ {4$\bar{5}$10} specimen deformed up to $\varepsilon = 0.7\%$ ($\sigma = 37.5$ MPa).

large than that of $\Sigma 21/\{4\bar{5}10\}$ boundary. This result may be related to the larger fracture stress of $\Sigma 7/\{4\bar{5}10\}$, because the zig-zag shaped boundary is expected to inhibit grain boundary sliding. It is thus considered that the $\Sigma 21/\{4\bar{5}10\}$ boundary undergoes sliding more easily than the $\Sigma 7/\{4\bar{5}10\}$ boundary.

These results indicate that not only the geometric parameter but also the atomic structures of the grain boundaries have to be considered to explain the differences in the mechanical strengths of the grain boundaries.

Figure 5 shows the experimental HRTEM images of the $\Sigma 7/\{4\bar{5}10\}$, $\Sigma 7/\{2\bar{3}10\}$, $\Sigma 21/\{4\bar{5}10\}$ and $\Sigma 21/\{2\bar{3}10\}$ boundaries viewed along the [0001] direction. White dots correspond to the Al columns in the present image conditions. From the HRTEM images, it was observed that tilt angles in ideal values shown in Table 1. In our previous studies,[31,32] static lattice simulations based on the ionic potentials were also performed for these grain boundaries to analyze the atomic structures at the grain boundary cores. The calculated structures with the lowest grain boundary energies were shown in Fig. 6. From close comparisons between the experimental images and the HRTEM simulation images based on the calculated atomic structures (see the insets in Fig. 6), it was confirmed that the calculated structures well agreed with the experimental images (Fig. 7). It can be seen from Fig. 6 that $\Sigma 7/\{4\bar{5}10\}$ boundary exhibits the relatively dense atomic arrangement at the core, whereas the core structures at the other boundaries have open spaces. Such differences in the core structures of the grain boundaries are expected to be closely related to their mechanical strengths shown in Fig. 3.

From the calculated structures, atomic densities at the grain boundaries were analyzed. Assuming that a particular grain boundary has a thickness of Δd as shown in Fig. 8(a), a rectangular grain boundary area with a volume of V_{gb} can be defined. In addition, Al and O ions were considered to be rigid ion spheres with radii of 0.053 nm and 0.140 nm,[34,35] respectively, and a volume occupancy v of ions (Al or O) within V_{gb} was calculated. For example, an Al atomic density ρ_{Al} can be represented by

$$\rho_{Al} = \frac{v_{Al}}{V_{gb}}. \quad (1)$$

Figure 8 shows the variations of (b) ρ_{Al} and (c) ρ_{Oxy} against Δd for the four kinds of the grain boundaries. It can be seen that atomic densities of the grain boundaries were different around the grain boundary cores. This is due to the differences in the core structures of the grain boundaries shown in Fig. 6. Especially, Al densities are very different in the range of $\Delta d < 0.2$ nm. In the case of $\Sigma 7/\{4\bar{5}10\}$, the ρ_{Al} and ρ_{Oxy} exhibited the largest values, which can be expected from the dense core structure in Fig. 6(a). At the same time the ρ_{Al} and ρ_{Oxy} for $\Sigma 21/\{2\bar{3}10\}$ showed the smallest values, which can be imaged from the open core structure shown in Fig. 6(d). For the calculated ρ_{Al} values at $\Delta d = 0.1$ nm, the

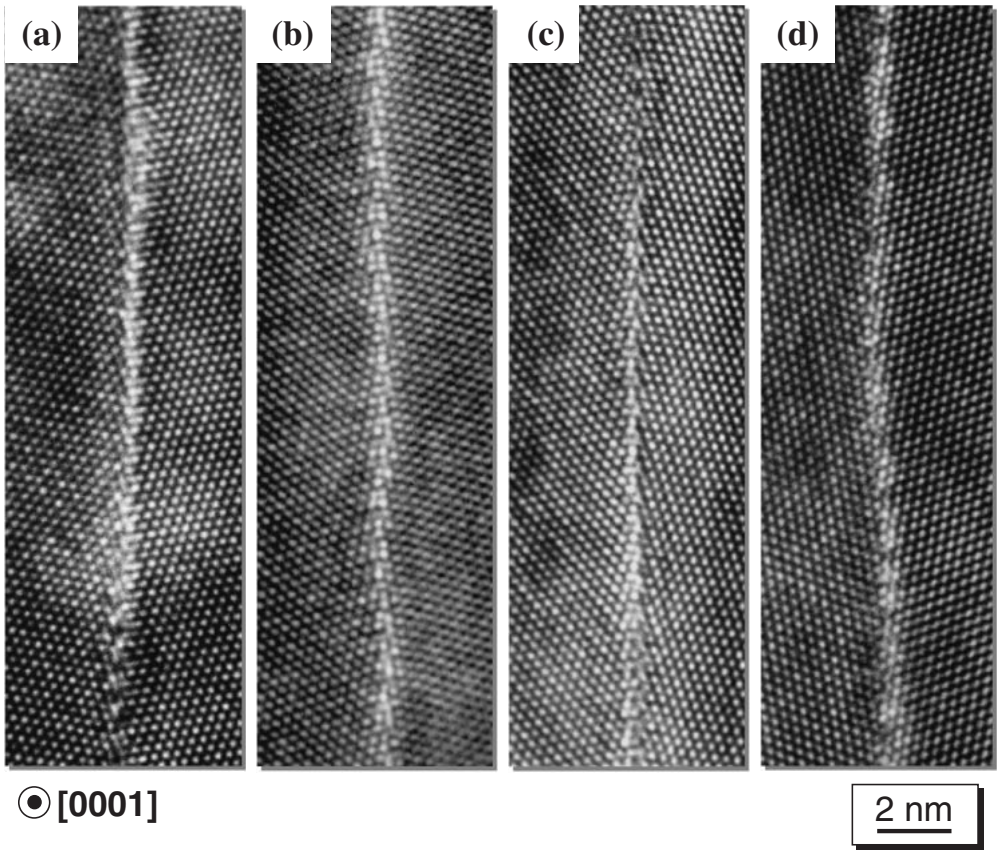

Fig. 5 HRTEM images of (a) $\Sigma 7$ $\{4\bar{5}10\}$, (b) $\Sigma 7$ $\{2\bar{3}10\}$, (c) $\Sigma 21$ $\{4\bar{5}10\}$ and (d) $\Sigma 21$ $\{2\bar{3}10\}$ specimens, in which the incident beam were set to parallel [0001] direction. White dots in the respective images correspond to the Al positions in the present observation conditions.

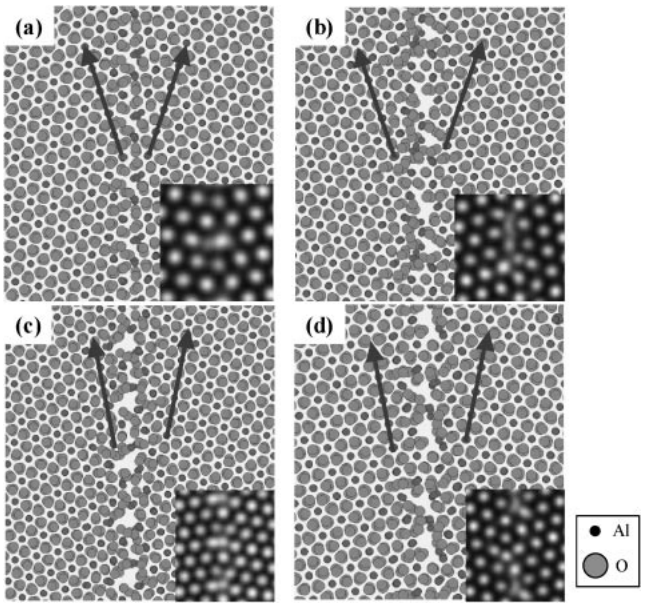

Fig. 6 The grain boundary atomic structures calculated for (a) $\Sigma 7$ $\{4\bar{5}10\}$, (b) $\Sigma 7$ $\{2\bar{3}10\}$, (c) $\Sigma 21$ $\{4\bar{5}10\}$ and (d) $\Sigma 21$ $\{2\bar{3}10\}$ respectively. The arrows indicate the $[1\bar{1}00]$ ((a), (d)), and $[11\bar{2}0]$ ((b), (c)) directions in the corundum structure. HRTEM image simulations obtained from the calculated structures are inset in the respective atomic models. Detailed simulation procedures used here are described in the previous papers.[30,31]

experimental fracture stresses in Fig. 3 were plotted in Fig. 9, in order to examine a relationship with the experimental fracture stresses. This is because Al diffusion has been considered to be a rate-controlling factor for the grain boundary diffusion in Al_2O_3 polycrystals.[36,37] It can be seen that as the ρ_{Al} value increases, the grain boundary fracture stresses of the grain boundaries become higher. There is a good correlation between the Al densities at the grain boundary cores and the mechanical strengths of the grain boundaries. It can be said, therefore, that the core structures of the grain boundaries play a significant role for determining their sliding resistances.

In this study, high-temperature compressive tests were conducted for the $\Sigma 7$ and $\Sigma 21$ boundaries with different grain boundary planes. It was found that these boundaries showed different sliding resistances, which were closely related to the core structures of the grain boundaries. So far, stability of grain boundaries tends to be understood by macroscopic degrees of freedom for the grain boundaries such as Σ values. However, the present results suggest that it is necessary to consider detailed atomic structures of the grain boundaries, in order to quantitatively clarify grain boundary properties.

4. Conclusion

Compressive mechanical tests were performed at a constant strain rate at 1450°C in air for the [0001] symmetrical

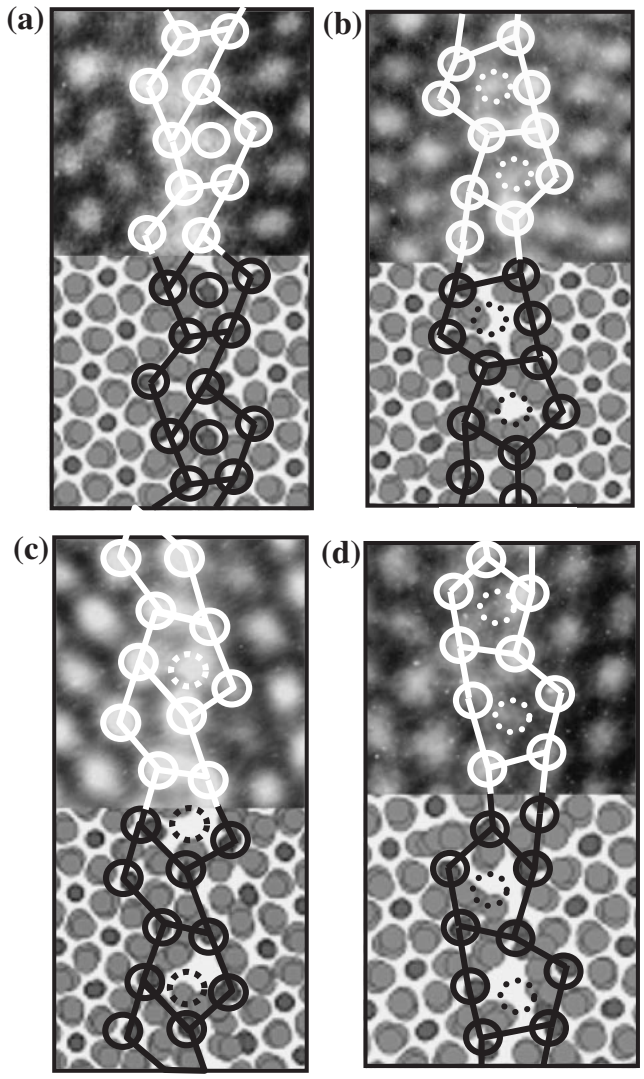

Fig. 7 HRTEM images and calculated atomic structures for (a) $\Sigma 7$ $\{4\bar{5}10\}$, (b) $\Sigma 7$ $\{2\bar{3}10\}$, (c) $\Sigma 21$ $\{4\bar{5}10\}$ and (d) $\Sigma 21$ $\{2\bar{3}10\}$ respectively.

tilt boundaries of $\Sigma 7/\{4\bar{5}10\}$, $\Sigma 7/\{2\bar{3}10\}$, $\Sigma 21/\{4\bar{5}10\}$ and $\Sigma 21/\{2\bar{3}10\}$ in Al_2O_3 bicrystals. The behaviors of the grain boundary sliding were discussed with the grain boundary core structures analyzed by HRTEM and atomistic simulations. The obtained results can be summarized as follows.

(1) By compressive tests, it was found that the $\Sigma 7/\{4\bar{5}10\}$ boundary exhibited the highest sliding resistance. In contrast, the other boundaries showed much smaller fracture stresses than $\Sigma 7/\{4\bar{5}10\}$, and thus the trend of the sliding resistances can not be easily explained by their Σ values.

(2) From the atomic structures at the grain boundary cores, the $\Sigma 7/\{4\bar{5}10\}$ boundary was found to have a relatively dense atomic arrangement, as compared to the other boundaries.

(3) The fracture stress of Al_2O_3 bicrystals was found to have a good correlation with the atomic densities at the grain boundary cores. This indicates that the detailed core structures play an important role for the sliding resistance of the grain boundaries.

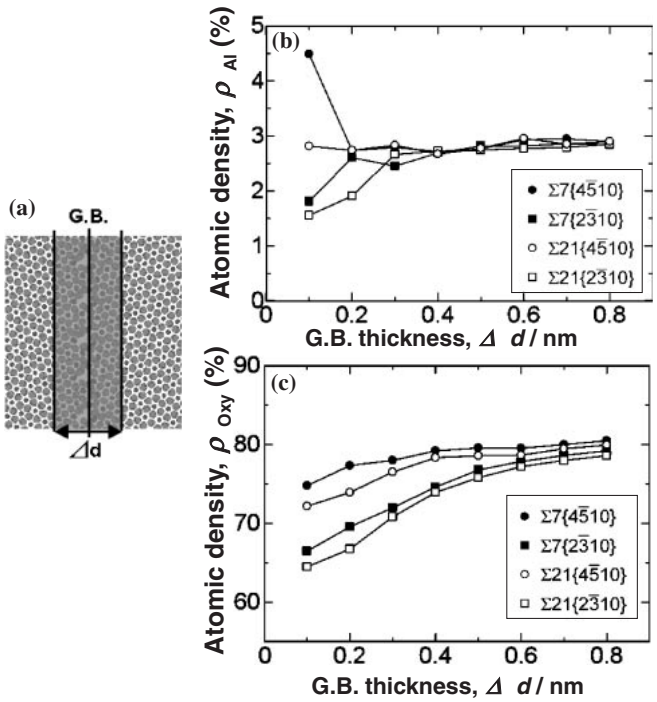

Fig. 8 (a) Schematic illustration indicating the definition of grain boundary thickness, and the relationship between G.B. thickness and densities of (b) Al and (c) O contained within the thickness.

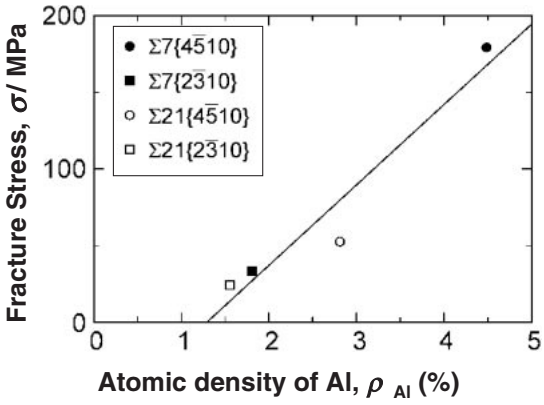

Fig. 9 Relationship between the Al atomic density and fracture stress for the respective grain boundaries.

Acknowledgements

This study was supported by a Grant-in-Aid for Scientific Research and Special Coordination Funds from the Ministry of Education, Culture, Sports, Science and Technology, and Japan Society of Promotion of Science (JSPS), Japan. The authors would like to express thanks to Dr. Gale for allowing us to use the GULP code.

REFERENCES

1) R. Raj and M. F. Ashby: Metall. Trans. **2** (1971) 1113–1127.
2) R. M. Cannon, W. H. Rhodes and A. H. Heuer: J. Am. Ceram. Soc. **63** (1980) 46–53.
3) H. Yoshida, K. Okada, Y. Ikuhara and T. Sakuma: Philos. Mag. Lett. **76** (1997) 9–14.
4) H. Yoshida, Y. Ikuhara and T. Sakuma: J. Mater. Res. **13** (1998) 2597–

2601.
5) J. Cho, M. P. Harmer, H. M. Chan, J. M. Rickman and A. M. Thompson: J. Am. Ceram. Soc. **80** (1997) 1013–1017.
6) T. Watanabe, M. Yamada, S. Shima and S. Karashima: Philos. Mag. A **40** (1979) 667–683.
7) R. Monzen, Y. Sumi, K. Kitagawa and T. Mori: Acta Metall. Mater. **38** (1990) 2553–2560.
8) A. D. Sheikh-Ali and J. A. Szpunar: Mater. Sci. Eng. A **245** (1998) 49–54.
9) C. Schmidt, M. W. Finnis, F. Ernst and V. Vitek: Philos. Mag. A **77** (1998) 1161–1184.
10) J. R. Hu, S. C. Chang, F. R. Chen and J. J. Kai: Mater. Chem. Phys. **74** (2002) 313–319.
11) D. G. Brandon, B. Ralph, S. Ranganathan and M. S. Wald: Acta Metall. **12** (1964) 814–821.
12) D. M. Saylor, A. Morawiec, B. L. Adams and G. S. Rohrer: Int. Sci. **8** (2000) 131–140.
13) W.-Y. Lee, P. D. Bristowe, Y. Gao and K. L. Merkle: Philos. Mag. Lett. **68** (1993) 309–314.
14) U. Dahmen, S. Paciornik, I. G. Solorzano and J. B. Vandersande: Int. Sci. **2** (1994) 125–136.
15) K. L. Merkle and D. J. Smith: Phys. Rev. Lett. **59** (1987) 2887–2890.
16) N. Shibata, T. Yamamoto, Y. Ikuhara and T. Sakuma: J. Electron. Microsc. **50** (2001) 429–433.
17) N. Shibata, N. Morishige, T. Yamamoto, Y. Ikuhara and T. Sakuma: Philos. Mag. Lett. **82** (2002) 175–181.
18) N. Shibata, F. Oba, T. Yamamoto, T. Sakuma and Y. Ikuhara: Philos. Mag. **83** (2003) 2221–2246.
19) T. Watanabe, Y. Ikuhara and T. Sakuma: J. Ceram. Soc. Jpn. **106** (1998) 888–892.
20) Y. Ikuhara, T. Watanabe, T. Saito, H. Yoshida and T. Sakuma: Mater. Sci. Forum. **294–296** (1999) 273–276.
21) Y. Ikuhara, T. Watanabe, T. Yamamoto, H. Yoshida and T. Sakuma: *Grain-Boundary Engineering in Ceramics-From Grain-Boundary Phenomena to Grain-Boundary Quantum Structures*, (American Ceramic Society, Westerville, OH, 2000) pp. 293–302.
22) P. R. Kenway: J. Am. Ceram. Soc. **77** (1994) 349–355.
23) F. R. Chen, C. C. Chu, J. Y. Wang and L. Chang: Philos. Mag. A **72** (1995) 529–544.
24) S.-D. Mo, W.-Y. Ching and R. H. French: J. Am. Ceram. Soc. **79** (1996) 627–633.
25) S. Fabris and C. Elsässer: Phys. Rev. B: Condens. Mater. **64** (2001) 1–10.
26) T. Höche, P. R. Kenway, H.-J. Kleebe and M. Rühle: J. Am. Ceram. Soc. **77** (1994) 339–348.
27) S. Nufer, A. G. Marinopoulos, T. Gemming, C. Elsässer, W. Kurtz, S. Kostlmeier and M. Rühle: Phys. Rev. Lett. **86** (2001) 5066–5069.
28) A. G. Marinopoulos and C. Elsässer: Acta Mater. **48** (2000) 4375–4386.
29) G. C. Hasson and C. Goux: Scr. Metall. **5** (1971) 889–894.
30) D. Wolf: Acta Metall. **37** (1964) 1983–1993.
31) K. Matsunaga, H. Nishimura, T. Saito, T. Yamamoto and Y. Ikuhara: Philo. Mag. **83** (2003) 4071–4082.
32) H. Nishimura, K. Matsunaga, T. Saito, T. Yamamoto and Y. Ikuhara: J. Am. Ceram. Soc. **86** (2003) 574–580.
33) J. D. Gale, GULP (General Utility Lattice Program), Royal Institution of Great Britain, London, U.K., 1993.
34) R. D. Shannon and C. T. Prewitt: Acta Cryst. B. **25** (1969) 925–946.
35) R. D. Shannon and C. T. Prewitt: Acta Cryst. B. **26** (1970) 1046–1048.
36) A. E. Paladino and R. L. Coble: J. Am. Ceram. Soc. **46** (1963) 133–136.
37) R. L. Coble: J. Appl. Phys. **34** (1963) 1679–1682.